RSC Advances

Silica Nanoparticles Densely Grafted with PEO for Ionomer Plasticization

Journal:	*RSC Advances*
Manuscript ID:	RA-ART-11-2014-015178.R1
Article Type:	Paper
Date Submitted by the Author:	08-Feb-2015
Complete List of Authors:	O'Reilly, Michael; University of Pennsylvania, Materials Science and Engineering Winey, Karen I.; University of Pennsylvania, Materials Science and Engineering

Silica Nanoparticles Densely Grafted with PEO for Ionomer Plasticization

Michael V. O'Reilly, Karen I. Winey*

Materials Science and Engineering, University of Pennsylvania, Philadelphia, PA 19104-6272

* Correspondence to: Karen I. Winey (winey@seas.upenn.edu)

Keywords: nanocomposite ionomer, PEO grafting, polymer electrolyte, lithium ion

ABSTRACT

A method for densely grafting poly(ethylene oxide) chains to the surface of silica is presented. The PEO-grafted nanoparticles (PEONPs) are dispersed in a PEO single-ion conductor to accelerate ion transport with an additive that is not molecular, oligomeric, or ionic. Grafting high molecular weight brushes to nanoparticles suppresses PEO crystallinity and lowers the glass transition temperature of the nanocomposite ionomers. Ionic conductivity can be improved by up to an order of magnitude at room temperature with increasing PEONP content while viscosity is reduced. Dielectric spectra corroborate the enhanced ionic conductivity as ion relaxation times decrease with PEONP content. The PEONPs are compared with bare silica nanoparticles (SNPs), which demonstrate more homogenous dispersion in the PEO ionomer than PEONPs. Good dispersion in the SNP nanocomposite ionomers results in viscosity improvements by up to 3 orders of magnitude, but reduces ionic conductivity by one order magnitude. PEONPs show potential as additives to other solid electrolytes, while SNPs enable a more robust electrolyte with modest conductivity penalty.

1. INTRODUCTION

In choosing an electrolyte for battery applications, high performance ion conductors typically come at the cost of structural rigidity. Significant and safe advances in battery capacity demand rigidity, conductivity, and electrochemical stability from their electrolytes.[1] Lithium-conducting polymer electrolytes offer advantages in rigidity and stability to attain higher energy densities over their liquid counterparts, but low molecular weight plasticizers and salts are typically required to elevate ionic conductivity to competitive levels.[2, 3] A variety of PEO/salt complexes have been studied for polymer electrolyte applications,[4-7] but they demonstrate high ionic conductivity and electrode polarization, because they are bi-ion conductors. For example, bulky anions, such as $TFSI^-$, contribute to charge transport in a Li^+ battery, but cannot be intercalated into an electrode. Single-ion conducting ionomers, where Li^+ is the only mobile charge carrier, are capable of cation transference numbers approaching 1.0.

PEO sulfoisophthalate ionomers (Figure 1) have been extensively studied as a function of temperature, PEO spacer molecular weight, ion content, and cation size.[8-14] These lithium ionomers with high ion content contain extensive ionic aggregation, causing slow ion dynamics. Electrode polarization analysis of dielectric spectroscopy data shows that less than 1% of Li^+ in the system are simultaneously contributing to conductivity.[8] *Ab initio* calculations conclude that the other > 99% exist in non-conductive ion states, such as pairs or quadrupoles.[15] Conductivity may be improved by lengthening the bridging PEO spacer to accelerate segmental dynamics, but crystallization impedes ion conduction at spacer molecular weights >1000 Da. Therefore, effort has been concentrated on increasing the number of simultaneously conducting ions by solvating them from their aggregated state. More recently, an oligomeric PEG (600 Da) plasticizer was

added to PEO and siloxane ionomers so as to enhance the segmental dynamics.[16, 17] These studies revealed that PEG plasticizer solvates ions, thereby improving conductivity.

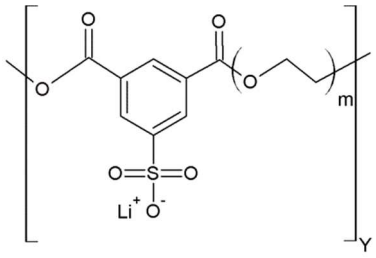

Figure 1. PEO/sulfoisophthalate ionomers neutralized with lithium, where *m* is adjustable, and dictates the molecular weight of the PEO spacer.

Nanocomposites are a viable pathway for providing both fast ion conduction and mechanical properties. Since the conduction mechanism is closely coupled with the segment dynamics of the polymer, high conductivity electrolytes tend to have low viscosities, and much research is focused on making membranes mechanically more robust. Adding solid nanofillers to polymer electrolytes is a well-studied field,[18-21] and a recent review by the Archer group[22] details significant advances in the last 25 years. Specifically, functionalizing nanoparticles with ligands designed for improved ion conduction is gaining momentum.[23-32] Yet, the introduction of filler interfaces makes understanding the fundamental ion transport mechanism in these hybrid systems even more complicated.

PEO-grafted silica doped with lithium salts were studied by Archer and coworkers,[26-28] who found widely tunable electrolyte viscosities without compromising ionic conductivity. Other studies of nanocomposite ionomers focus on functionalizing nanoparticles to include ionic salts. Chinnam and Wunder functionalized POSS with PEO and $LiBF_4$ salt, and observed conductivities as high as 10^{-3} S/cm at elevated temperature, as well as improved Li^+ transference

numbers.[23] Two studies from the Fedkiw group are of particular interest for fabricating conducting nanocomposites.[30, 32] Zhang *et al.* dispersed lithiated nanoparticles in PEG dimethyl ether and found enhanced ionic conductivity with nanoparticle loading content.[30] In a more recent study, Zhang *et al.* grew ionic polymers from the surface of silica by ATRP, dispersed them in propylene carbonate, and observed ionic conductivity greater than 10^{-5} S/cm; formidable for a single-ion conductor.[32]

Here, we present a comparison between two nanoparticle fillers with vastly different interfacial properties mixed with a PEO-based ionomer. One set of nanoparticles are functionalized with PEO to facilitate ion transport, and the second set are bare silica nanoparticles with hydroxyl surfaces. Ionic species are neither tethered to the nanoparticles as described above, nor are excess salts or plasticizers added to the nanocomposite. Specifically in this study, we target enhancing the conducting ion content, mobility, and conductivity of lithium ions by plasticizing our single-ion conducting polymer with PEO-grafted nanoparticles. Comparisons are drawn with nanocomposites prepared with bare silica, where no benefit from filler content is expected, but enhancements in ionomer viscosity can be achieved. The breadth of prior studies on the PEO single-ion conductor provide an excellent foundation for exploring the balance between ion transport and viscosity in nanocomposites where we find that enhanced segmental dynamics improves conducting ion content and ion mobility.

2. EXPERIMENTAL METHODS

2.1. Materials

Colloidal silica was acquired from Nissan Chemical (Organosilicasol MT-ST, 30 wt% silica in methanol, 10-15 nm diameter). Poly(ethylene glycol) methyl ether (PEO5k, average

M_n = 5,000 Da), poly(ethylene glycol) (PEG600, average M_n = 600 Da), dimethyl 5-sulfoisophthalate sodium salt (DM5SIS, 98%), lithium chloride (LiCl, 99%), sodium hydride (NaH, 60% dispersion in mineral oil), butyltin hydroxide oxide hydrate (97%), tetrahydrofuran (THF, anhydrous, 99.9%), ethylene glycol (>99%), and toluene (anhydrous, 99.8%) were purchased from Sigma Aldrich. 3-Bromopropyltrichlorosilane and hexamethyldisilazane (HMDS) were purchased from Gelest, and used as received.

2.2. Synthesis of PEO600 100% Li Ionomer

The single-ion conducting PEO ionomer used in this study was synthesized by a modified version of a method described previously, and is illustrated in Figure 2(a).[8] 12 g of PEG600 diol, 5.9 g DM5SIS, and 19 mg of butyl tin hydroxide oxide were pre-dried to eradicate water and added to a flask at 25 °C under argon flow. The temperature was raised to 210 °C while stirring and a vacuum was pulled to remove byproduct methanol. Throughout the reaction, the viscosity increased significantly. After 7 hours, the temperature was lowered to 160 °C and a few drops of ethylene glycol were added. The vessel was flushed with argon and brought to room temperature. The resultant PEO-sulfonated isophthalate ionomer was dissolved in 50 ml D.I. water to which a stoichiometric excess of LiCl salt was added to ion exchange the ionomer from Na^+ to Li^+. The final ionomer was dialyzed (1000 Da MWCO tubing, Spectrum Labs) against D.I. water to remove ions and impurities until constant conductivity was reached. Ionomer chemical structure was confirmed by proton NMR. Number and weight averaged molecular weights were measured to be 6120 Da and 9640 Da, respectively, with a PDI of 1.57 by size exclusion chromatography.

2.3. Grafting Silica Nanoparticles with PEO Brushes

The colloidal silica nanoparticles (SNPs) were first solvent exchanged by adding 11 g of colloid in methanol to 40 ml of anhydrous toluene at 100°C while stirring for 8 hours. The suspension was then sonicated in a water bath until the suspension transitioned from turbid to transparent. The suspension was immediately transferred to an oil bath set to 70°C and placed under Argon flow. A previously prepared suspension of 4 ml 3-bromopropyltrichlorosilane in 10 ml anhydrous toluene was added drop-wise to the stirring dispersion of nanoparticles, and the reaction continued for 17 hours before lowering the temperature. The bromopropyl-functionalized nanoparticle suspension was precipitated into acetone, and excess solvent was pipetted off until only 100 ml of solvent remained. The suspension was pelletized by centrifugation and re-suspended in anhydrous THF three times to wash out HCl byproduct and unreacted silane.

A well-dried, argon-filled flask was charged with 10 ml of anhydrous THF and 0.2 g NaH (60% in mineral oil) while stirring in an ice bath. 10 g of pre-dried PEO5k was dissolved in 35 ml of anhydrous THF by heating and stirring. NaH and PEO5k quantities were used in 100x excess of the stoichiometric quantity of grafted silane for maximum grafting density. The PEO5k solution was dripped slowly into stirring NaH/THF and allowed to react for 1 hour while the strong base deprotonated the hydroxyl of the PEO5k. 0.24 g bromopropyl silica dispersed in 8 ml of anhydrous THF was dripped slowly into the vessel and the reactants were allowed to react for 1 hour on ice, and 3 hours at room temperature. The reactants were visually white and opaque with elevated viscosity due to some of the excess PEO5k crashing out of THF near 0°C, but after approximately 30 minutes the viscosity had reduced significantly. Upon completion of the reaction, the THF was removed under argon flow, and the PEO-grafted nanoparticles

(PEONPs), excess reactants, and byproducts were dissolved in D.I. water. The suspension was dialyzed with 10 kDa MWCO dialysis tubing (Fisher Scientific) in D.I. water until the dialysate was pure. The resulting suspension was dried and PEONPs recovered. The functionalization and final product are illustrated in Figure 2(b).

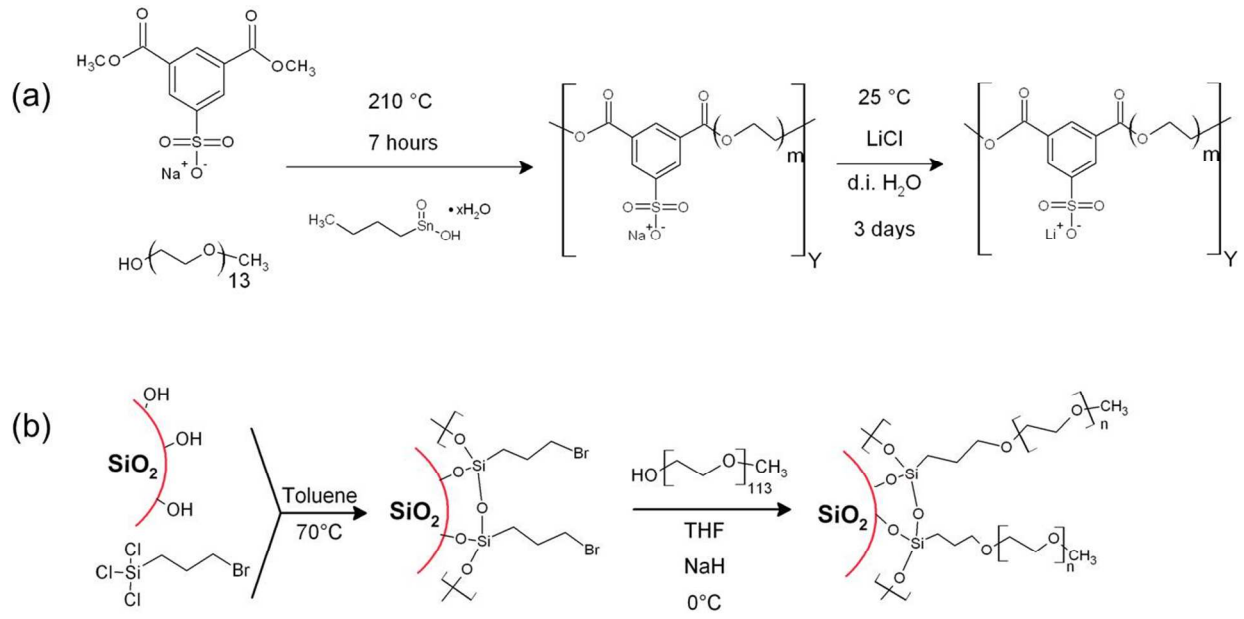

Figure 2. (a) PEO600/sulphoisophthalate Na ionomer polycondensation reaction and ion exchange to the Li neutralized form. **(b)** Two-step functionalization of colloidal silica nanoparticles with PEO5k by silane condensation and nucleophilic substitution.

2.4. Nanocomposite Fabrication

Nanocomposites were fabricated at varying weight percentages of modified nanoparticles, and are named *F*NP-*z*, where *F* is the functionality type (PEO or S (silanol)) and *z* is the weight percent of nanoparticles, Table 1. The weight percentages reflect the total weight of the grafted particles, thus at a fixed weight percent the relative number of nanoparticles per unit volume varies between functionality type. Ionomer and nanoparticles were dispersed in methanol in separate vessels by vigorous stirring, followed immediately by intermixing and

casting. Nanocomposites were drop-cast onto hot glass substrates set just below the boiling point of the casting solvent followed by extensive drying in a vacuum oven at 70 °C for > 48 h.

Table 1. Nanocomposite and blend compositions with PEO600 100% neutralized Li ionomer, their glass transition temperatures and ionic conductivities at 30 °C.

Sample	Filler	Filler wt%	T_g (°C)	σ_{DC} @ 30 °C (10^{-8} S/cm)
PEO600 Li	-	0	-13	4.5
SNP-10	Bare silica NP	10	-14	3.9
SNP-20	Bare silica NP	20	-13	0.45
SNP-35	Bare silica NP	35	-13	0.24
PEONP-10	PEONP	10	-19	6.9
PEONP-20	PEONP	20	-26	14
PEONP-27	PEONP	27	-25	17
PEONP-35	PEONP	35	-32	21
PEO-5	PEO5k	5	-13*	6.9
PEO-10	PEO5k	10	-12*	8.2
PEO-20	PEO5k	20	-13*	7.7

*PEO melting and crystallization peaks also detected

2.5. Thermal Analysis

Approximately 10 mg of dried, functionalized silica nanoparticles were measured for weight loss by a TA Q600 thermal gravimetric analyzer (TGA) at a heating rate of 5 °C/min up to 600 °C after each synthetic step to determine grafting density. The final, dried nanocomposites were characterized with a TA Q2000 differential scanning calorimeter (DSC). Samples (5-10 mg) in hermetically sealed aluminum pans were subjected to a heat-cool-heat cycle with equilibrations at 80 °C and -80 °C at a heating rate of 10 °C/min. The glass transition temperature, T_g, was defined as the midpoint of the heat flow step during the second heating sweep.

2.6. X-ray Scattering

Prior to X-ray scattering experiments, samples were placed on 50 μm thick ruby mica discs and dried in vacuum at 70°C for at least 24 hours. The samples were stored in vacuum until the transfer to the X-ray chamber to minimize moisture exposure. Cu Kα X-rays are generated by a Nonius FR 591 rotating-anode operating at 40 kV and 85 mA. The X-rays are collimated by an Osmic Max-Flux optic and three pinholes in an evacuated beamline, and collected by a Bruker Hi-Star multi-wire detector. Sample-to-detector distances of 11 cm and 150 cm were used for WAXS and SAXS data, respectively. Reduction of the 2D scattering patterns and SAXS fitting was completed with *Datasqueeze* software.[33] The background from a blank mica disc was subtracted at a ratio such that the slope of the data in the Porod regime was zero on an $I(q)\cdot q^4$ vs. q plot.

2.7. Dielectric Relaxation Spectroscopy (DRS)

Dielectric measurements were made with a Novocontrol GmbH Concept 40 broadband dielectric spectrometer by applying a 0.1 V AC voltage. Nanocomposite ionomers were dried at 80 °C for more than 48 hours under vacuum on polished brass electrodes to eradicate solvent and air bubbles from the sample. Two 50 μm glass fiber spacers defined the constant sample thickness and were used to support a top 10 mm polished brass electrode. Before starting the experiment, samples were annealed at 120 °C in nitrogen atmosphere for one hour. Frequency sweeps from 10^7 Hz to 10^{-2} Hz were conducted isothermally in step sizes of 10 °C or 5 °C down to 0 °C.

2.8. Electron Microscopy

Bright field scanning transmission electron microscopy (BFSTEM) images were collected on a JEOL 7500 FEG high resolution scanning electron microscope set to an accelerating voltage of 15 kV and current of 20 μA. Electron transparent samples were spun cast from 2 wt% methanol solutions of nanocomposite onto carbon-coated copper grids. Carbon-coated grids were plasma cleaned with hydrogen and oxygen to render the casting surface hydrophilic. Film thicknesses of approximately 70 nm were determined by elipsometry of films cast on silicon wafers with identical coating conditions.

2.9. Dynamic Light Scattering (DLS)

Solutions of 0.1 wt% PEONPs and SNPs were prepared in methanol by vigorous stirring. Suspensions were passed through 200 nm syringe filters and collected in disposable polystyrene cuvettes. Five measurements were averaged to determine the hydrodynamic diameter on a Malvern Zetasizer Nano-S at 25 °C.

2.10. Rheology

Viscoelastic measurements were conducted on an Advanced Rheometrics Expansion System ARES-LS1 rheometer (Rheometric Scientific) equipped with 7.9 mm diameter parallel plates under nitrogen atmosphere. Samples were dried in vacuum for >24 hours at 80 °C prior to measurements. Samples were further dried in the ARES-LS1 at 120 °C for one hour to eradicate water absorbed during sample transfer and to ensure good sample contact with the plates. Frequency sweeps from 10^2 to 10^{-2} Hz were conducted at 30 °C, 50 °C, 70 °C, and 90 °C. Time-temperature superposition was applied for all nanocomposites with a reference temperature of 50

°C. Thermal reproducibility was verified by re-measuring the viscoelastic response at the reference temperature upon completion of the temperature sweep.

3. RESULTS AND DISCUSSION

3.1. PEO Ionomer Morphology

The matrix for our nanocomposite single-ion conductors in this work is a PEO-based ionomer with an alternating PEO/sulfoisophthalate polymer architecture, and has been extensively characterized previously.[8-11] Our modifications to the ionomer synthesis have increased the number average molecular weight from 4.7 kDa to 6.1 kDa.[8] This increase in molecular weight corresponds to a few extra ionic groups per chain, increasing the number of physical cross-links per chain and increasing viscosity without changing T_g. The morphology of the PEO600 100% Li ionomer shows two main features in X-ray scattering representative of amorphous PEO scattering at q = 14 nm^{-1} (no crystallinity), and ionic aggregation at q = 2.7 nm^{-1} (Figure 3). This is consistent with earlier reports on the lower molecular weight ionomer.[10] This model ionomer is ideal for studies attempting to improve ion transport by facilitating ion dissociation due to the high percentage of arrested ions in ionic aggregates.

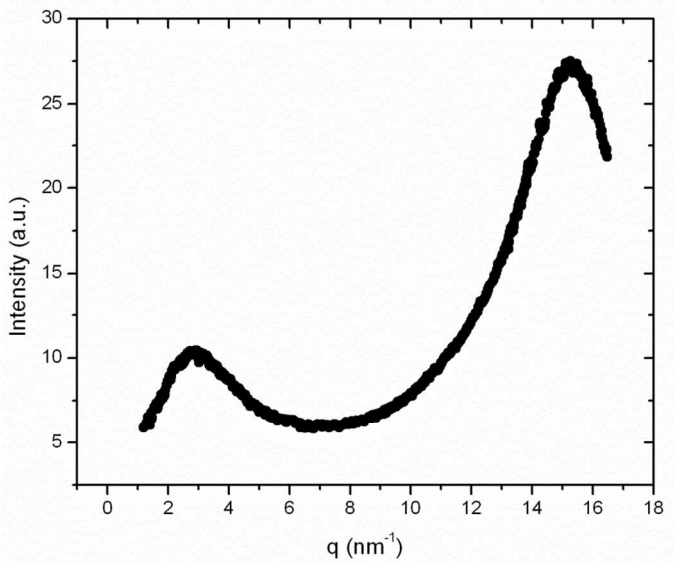

Figure 3. Wide angle X-ray scattering of PEO600 100% Li ionomer at 25 °C.

3.2. Nanocomposite Single-Ion Conductors

The trichloro functionality of the bromopropylsilane linker allows for a high (multi-layer) grafting density of silanes to maximize the number of PEO5k grafts on the NPs. The number density of leaving groups (Br) on the silica particles was calculated to be 1.9 functionalities/nm^2 by TGA. After reaction with PEO5k the grafting density was found to be remarkably high, with 1.5 chains per nm^2 as determined by TGA, while the primary hydrodynamic nanoparticle diameter increased from 21 nm to 58 nm with the addition of the PEO brush (by DLS). This high grafting density is consistent with a dry polymer brush thickness of 5-10 nm as measured from representative STEM images, Figure 4a. Further qualitative evidence of successful PEO grafting is how the NPs suspend in water, transitioning from stable (bare silica), to unstable (bromopropyl functionality), to stable once more (PEONPs).

The synthesis for PEONPs is adaptable for any molecular weight of PEO, and grafting density can be adjusted based on reaction concentrations. Early studies on grafting PEO to silica

employed the esterification of silanol with terminating hydroxyls of PEO to form an unstable Si-O-C bond.[34, 35] Our study circumvents the instability by condensing a stable silane linker to silanol. The brush molecular weight of 5 kDa was selected for its similarity to the total molecular weight of the PEO ionomer used as the matrix of these nanocomposites (6.1 kDa). Previous studies on polymer-grafted nanoparticles dispersed in a miscible polymer matrix found that nanoparticle dispersion is governed by the ratio of the matrix molecular weight (P) to brush molecular weight (N).[36-39,40, 41] When P is sufficiently larger than N, nanoparticles aggregate largely due to entropic penalties producing minimal interpenetration between the brush and matrix, namely the dry brush state. Nanoparticle dispersion transitions to a more homogeneous state when P and N are comparable and the matrix chains can swell the grafted chains to form the wet brush state. The exact P/N transition varies depending on the polymers, molecular weights, nanoparticle diameter, and grafting densities of the system. The present study deviates from previous studies is a few important ways, which will likely affect the degree of interpenetration between the matrix and brush: (1) the matrix and grafted polymers have low molecular weights, (2) the grafting density is very high, leading to a very extended chain conformation near the surface of the nanoparticle, and (3) the matrix is a PEO ionomer with extensive physical crosslinking, such that while the PEO brush is chemically similar to the PEO ionomer, it is devoid of ion content.

Figure 4(b) and (c) shows the dispersion quality of nanoparticles in spin cast ionomers as observed by BFSTEM, and these images are indicative of all nanocomposite compositions. The bare silica nanoparticles disperse well in the PEO matrix due to stabilization by hydrogen bonding and ionic interactions between hydroxylated silica surfaces and the PEO ionomer. The PEONPs, on the other hand, show poor dispersion in the PEO ionomer.

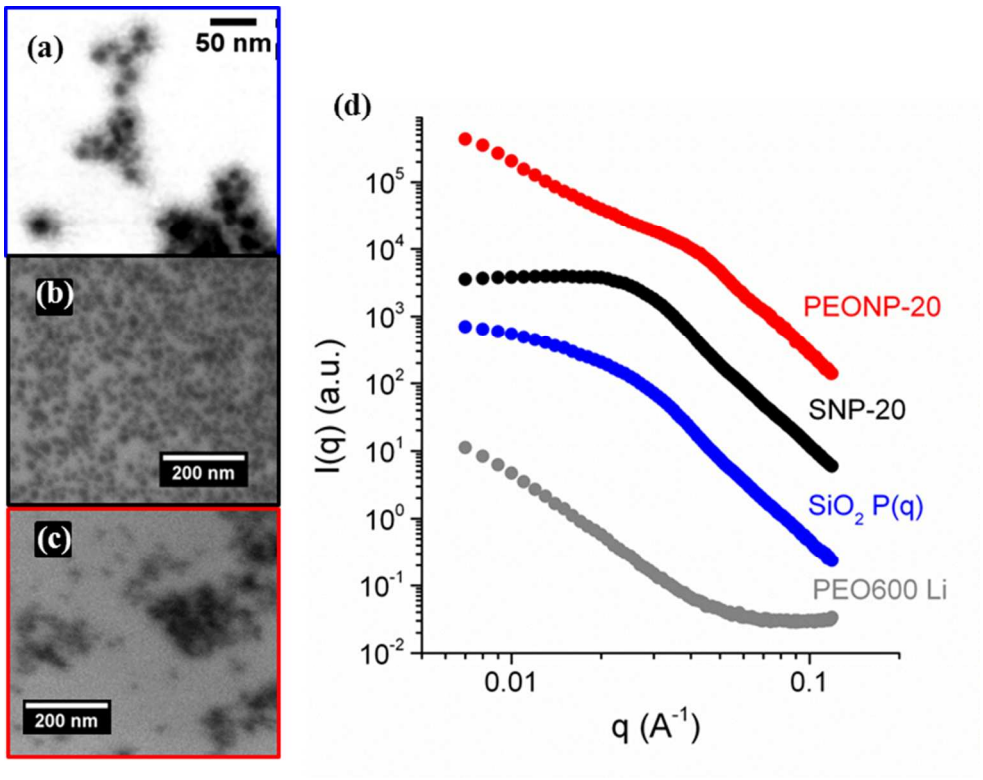

Figure 1. BFSTEM images of **(a)** drop-casted PEONPs (no polymer matrix), **(b)** SNP-20 nanocomposite, and **(c)** PEONP-20 nanocomposite. Thin films (~70 nm) were spin cast on ultrathin carbon support films. **(d)** Small angle X-ray scattering of SNP-20 and PEONP-20 nanocomposite ionomers, along with silica form factor and neat ionomer scattering for comparison. The ionomer scattering has been subtracted from the nanocomposite scattering. Curves have been shifted vertically for clarity.

The findings from BFSTEM are supported by X-ray scattering. The SAXS data for the neat ionomer and a dilute suspension of silica colloid in methanol are shown in Figure 4(d). The nanoparticle form factor scattering, P(q), is broad and does not demonstrate any scattering minima, owing to the polydispersity of the nanoparticles. The SAXS spectrum for the neat ionomer was subtracted from the SNP and PEONP nanocomposites to reveal scattering from the nanoparticles. Between 0.07 Å^{-1} < q < 0.12 Å^{-1}, the scattering data from both nanocomposites have a slope of -4, consistent with the Porod scattering regime for spherical particles. The small angle upturn between 0.007 Å^{-1} and 0.02 Å^{-1}, the PEONP-20 SAXS data indicates interaggregate

nanoparticle scattering at length scales greater than 30 nm (Figure 4(d)). Contrariwise, the well-dispersed nature of bare silica in the ionomer demonstrates a plateau at small angle, indicating no large scale correlation lengths.

The 10-15 nm nanoparticle diameter was selected to provide a high silica surface to volume ratio. Ideally, well-dispersed PEONPs would take full advantage of the plasticized interface between the nanoparticle and ionomer by lowering the glass transition temperature and boosting mobility and conducting ion concentration. Despite the comparable matrix (6.1 kDa) and brush (5 kDa) molecular weights and chemical structures of the matrix and brush, the PEONPs may not disperse well for several reasons. First, extensive ionic aggregation in the ionomer matrix persists in the presence of PEO brushes, because ionic aggregates are more stable than ether oxygen-solubilized lithium. Second, the high grafting density on the PEONPs produces extended chain conformations that entropically limit the penetration of the ionomer in the brush. Finally, the dense PEO brush replaced surface hydroxyls that favorably interacted with the matrix ionomer.

3.3. Thermal and Dielectric Relaxations

Glass transition temperatures of SNP and PEONP nanocomposites are reported in Figure 5. We observe a plasticization effect as PEONPs are incorporated into the ionomer matrix. The low T_g of the PEO brushes and the excess free volume provided by chain ends increases the segmental mobility at PEONP/matrix interfaces. The T_gs of the SNP nanocomposites are constant across all compositions, as chains associated with the hydroxylated silica surface do not contribute to the segmental relaxation process. Thus, the T_g is representative of the ionomer matrix independent of SNP concentration. For comparison, the PEO600 100% Li ionomer was

blended with various compositions of PEO5k oligomer. The tendency for PEO5k to crystallize causes phase separation of the two components, so that the ionomer glass transition temperature is independent of PEO5k concentration. Our study demonstrates that PEO-grafted silica nanoparticles provide a means of mixing high molecular weight, ion-solvating PEO with a single-ion conductor while suppressing immiscible, non-conducting, crystalline phases of PEO. Maitra *et al*. studied the thermal properties of PEO-grafted silica and came to a similar conclusion that tethering PEO to silica nanoparticles reduces the percent crystallinity of the grafted polymer.[42]

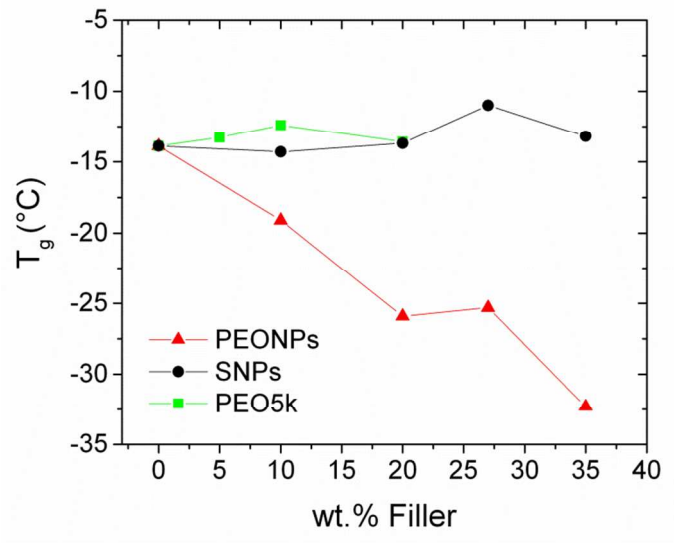

Figure 2. DSC glass transition temperatures *versus* filler weight percent for PEONP nanocomposites, SNP nanocomposites, and PEO5k/ionomer blends.

The neat PEO600 100% Li ionomers exhibit two relevant relaxations in dielectric relaxation spectroscopy within the frequency window of 10^{-2}-10^{7} Hz and over a temperature range from 0-120 °C.[9] The α relaxation appears at high frequency and is representative of segmental relaxation of the PEO spacers. The α_2 relaxation occurs at lower frequency than the α

process, but higher frequency than electrode polarization, and represents the timescale for ionic rearrangement of pairs, triplets, quadrupoles, and higher order aggregates. [9]

Typically, the α and α_2 processes can be observed in the dielectric loss spectra. But in our high ion content ionomer, ionic conductivity dominates the mid-frequency range and obscures the signal with a slope of -1. Thus, we use a derivative formalism of the dielectric storage to resolve these relaxations:[43]

$$\varepsilon_{der}(\omega) = -\frac{\pi}{2}\frac{\partial \varepsilon'(\omega)}{\partial (ln\omega)} \quad (1)$$

where ω is the angular frequency. The derivative of the storage modulus approximates the loss modulus in the absence of ionic conductivity. Figure 6 shows ε_{der} as a function of angular frequency and temperature in 10 °C steps for the neat PEO600 100% Li ionomer. The dominant feature is the electrode polarization (EP) peak that shifts from 10^3 rad/s at 120 °C to a low frequency point out of range at 0 °C. The α and α_2 relaxations are broader and weaker than EP, and are convoluted with one another at higher frequencies, shifting to lower frequencies simultaneously with EP as temperature is reduced. Approaching 0 °C, it is possible to resolve the β process (PEO chain twisting) at the highest accessible frequencies.

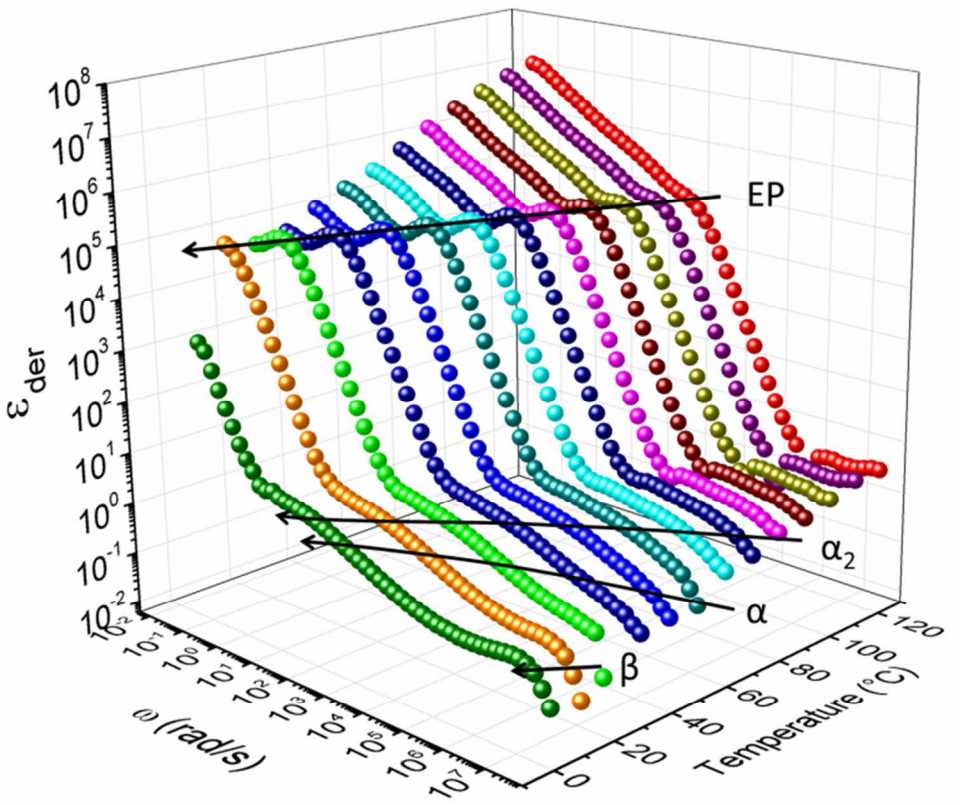

Figure 3. Representative derivative dielectric (ε_{der}) spectra of neat PEO600 Li ionomer from 0 °C to 120°C in 10°C increments. Arrows label the approximate temperature response of four relaxation processes.

Derivative dielectric spectra for each nanocomposite at 30 °C are fit with a sum of one power law and two Havriliak-Negami (HN) functions (Eq. 3)[43, 44] to capture EP and the α and α_2 relaxations, respectively:

$$\varepsilon *_{HN}(\omega) = \frac{\Delta\varepsilon}{[1 + (i\omega\tau_{HN})^{a}]^{b}} \qquad (2)$$

$$\frac{\partial \varepsilon'_{HN}}{\partial(ln\omega)} = -\frac{ab\Delta\varepsilon(\omega\tau)^a \cos[\frac{a\pi}{2} - (1+b)\theta_{HN}]}{[1 + 2(\omega\tau)^a \cos\left(\frac{\pi a}{2}\right) + (\omega\tau)^{2a}]^{(1+b)/2}} \quad (3)$$

where θ_{HN} = arctan [sin(πa/2)/(($\omega\tau$)$^{-a}$ + cos(πa/2))], Δε is the dielectric relaxation strength, *a* and *b* are shape parameters constrained so that *ab* ≤ 1, and τ_{HN} is the relaxation time. It is not possible to fit these spectra with a single HN function.

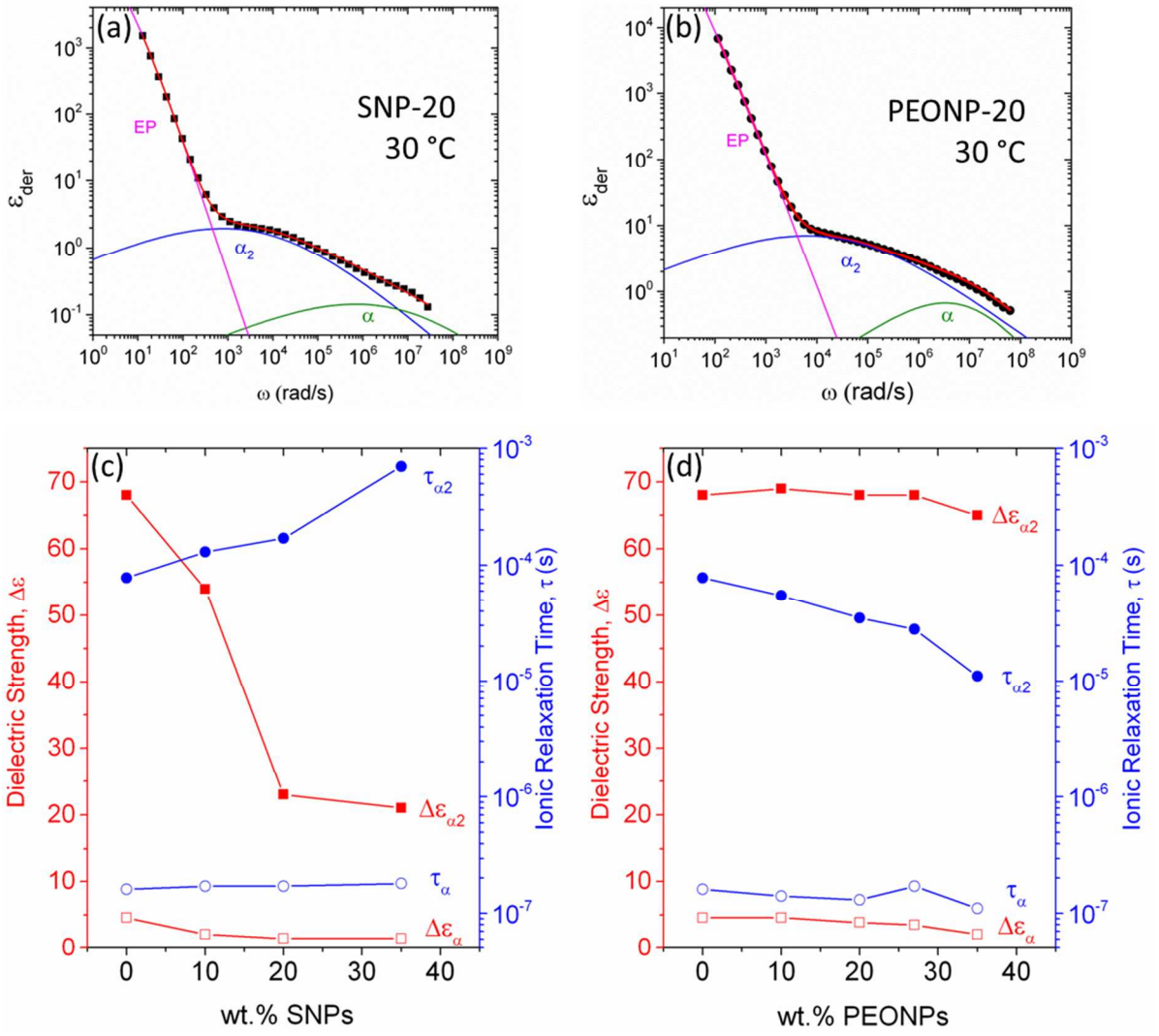

Figure 4. Derivative dielectric spectra taken at 30 °C of **(a)** SNP-20 and **(b)** PEONP-20, fit with a power law and two Havriliak-Negami relaxations. Dielectric strengths (Δε, red) and relaxation times (τ, blue) at 30 °C for the α (open) and α_2 (filled) processes are also compared for **(c)** SNPs and **(d)** PEONPs as a function of nanoparticle composition.

Table 2. Havriliak-Negami fitting parameters at 30 °C for dielectric strength (Δε) and relaxation time (τ) of the segmental (α) and ionic rearrangement (α_2) relaxations.

Sample	$\Delta\varepsilon_\alpha$	τ_α (μs)	$\Delta\varepsilon_{\alpha 2}$	$\tau_{\alpha 2}$ (μs)
Neat ionomer	4.6	0.16	68	78
SNP-10	2.1	0.17	54	130
SNP-20	1.5	0.17	23	170
SNP-35	1.5	0.18	21	700
PEONP-10	4.6	0.14	69	55
PEONP-20	3.9	0.13	68	35
PEONP-27	3.5	0.17	68	28
PEONP-35	2.1	0.11	65	11

Dielectric strengths and relaxation times are compared at 30 °C, so that the relaxations were resolvable without interference from EP. Figure 7(a) and (b) show the ε_{der} fit for SNP-20 and PEONP-20, respectively. The dielectric strengths ($\Delta\varepsilon_\alpha$ and $\Delta\varepsilon_{\alpha 2}$) and relaxation times ($\tau_\alpha$ and $\tau_{\alpha 2}$) for all nanocomposites are listed in Table 2. The dielectric strength of the α process is approximately an order of magnitude smaller than that of the α_2 process owing to the strong dipoles associated with the ionic groups compared with weaker PEO segment dipoles. More interestingly, the trends for α_2 relaxation strengths and times for the two varieties of nanoparticle as a function of composition are compared in Figures 7(c) and 7(d). At high SNP content, $\Delta\varepsilon_{\alpha 2}$ is reduced by a factor of three compared to the neat ionomer. Hydrogen bonding and ionic interactions between surface silanols, ether oxygens, and ion pairs arrest the PEO ionomer at the nanoparticle surface, preventing lithium solvation and dipole relaxation. The $\Delta\varepsilon_{\alpha 2}$ reduction suggests ion rearrangement is less frequent in bare silica nanocomposites than the neat ionomer. Conversely, $\Delta\varepsilon_{\alpha 2}$ for PEONP nanocomposites is independent of nanoparticle composition. Ionic relaxation contributions to the dielectric constant are independent of PEONP weight fraction,

indicating that ions are at least equally mobile in the nanocomposite when compared with the neat ionomer. This composition-insensitive dielectric strength is even more significant when considering the ion content of the nanocomposite is diluted by the non-ionic PEONPs, requiring a larger percentage of total ions to be involved in ionic rearrangement. This rearrangement has implications on DC conductivity at room temperature, see section 3.4.

The time scales for ionic relaxations ($\tau_{\alpha 2}$) are 2-3 orders of magnitude slower than PEO segmental relaxations (τ_{α}) due to strong Coulombic attractions immobilizing ionic species. The relaxation time for ionic rearrangement in SNP nanocomposites and PEONP nanocomposites show opposite behaviors. Ions relax more slowly with increasing SNP content, leading to less frequent rearrangement, as consistent with the reduced dielectric strength values. Meanwhile, PEONPs accelerate the ionic relaxation process by a factor of 7 at the highest PEONP content, thereby maintaining a strong dielectric strength despite lower ion content.

Finally, we expect that both electrode polarization and nanoparticle surface polarization occur in these materials, but we do not observe the latter in this frequency and temperature window. This type of nanoparticle interfacial polarization would be heavily dependent on nanoparticle concentration. As the surface area of nanofiller is increased, we would expect to see an increase in the total dielectric strength of ε_{der}, which is not observed. Therefore, there is no evidence of observable interfacial polarization in our nanocomposites under the presented conditions.

3.4. Ion Transport Properties

The electrode polarization (EP) model[45, 46] may be applied to single-ion conducting polymers to extract the fundamental components of DC ionic conductivity:

$$\sigma_{DC} = e\mu p \tag{4}$$

Ion mobility (μ), the simultaneous conducting ion concentration (p), and monovalent ion charge (e) are separated by treating the system as if lithium is the only contributor to conductivity. The validity of the electrode polarization model is founded on the immobilization of the sulfonate anion by covalent tethering to the polymer backbone. DC conductivity measurements are recorded from the linear portion of the dielectric loss modulus, and taken to be the frequency-independent conductivity in the AC electric field.

The DC conductivity is used to define two relevant time scales to our calculation of mobility and conducting ion concentration:

$$\tau_\sigma = \frac{\varepsilon_s \varepsilon_0}{\sigma_{DC}} \tag{5}$$

$$\tau_{EP} = \frac{\varepsilon_{EP} \varepsilon_0}{\sigma_{DC}} \tag{6}$$

τ_σ is the time scale for ion conduction and τ_{EP} is the time scale for electrode polarization, where ε_s is the static dielectric constant before electrode polarization, ε_{EP} is the dielectric constant after electrode polarization, and ε_0 is the dielectric constant of vacuum. Values for these time scales are obtained by fitting the loss tangent, tanδ, with a Debye relaxation:

$$tan\delta = \frac{\omega \tau_{EP}}{1 + \omega^2 \tau_\sigma \tau_{EP}} \tag{7}$$

From the fit of the loss tangent with Equation 7, we can calculate conducting ion concentration (p) and ion mobility (μ):

$$p = \frac{1}{\pi l_B L^2}\left(\frac{\tau_{EP}}{\tau_\sigma}\right)^2 \quad (8)$$

$$\mu = \frac{\sigma_{DC}}{ep} \quad (9)$$

$$l_B = \frac{e^2}{4\pi\varepsilon_0\varepsilon_s kT}\left(\frac{\tau_{EP}}{\tau_\sigma}\right)^2 \quad (10)$$

where l_B is the Bjerrum length and L is the sample thickness. However, the mobility and conducting ion concentration are actually independent of the electrode separation distance due to the proportionality between τ_{EP} and L, as explained previously.[47]

The DC conductivity is plotted as a function of inverse temperature in Figure 8(a). The conductivity demonstrates non-linear inverse temperature response across the entire range, suggesting that the mode for ion transport is assisted by segmental relaxation of the ionomer PEO spacer. With increasing PEONP content, the room temperature conductivity methodically increases, with a maximum improvement of one order of magnitude. At high temperature, the conductivity collapses to a PEONP concentration-independent value. An inverse relationship between dielectric constant and temperature causes PEO to be less effective at ion solvation at high temperature. A previous morphology study on the PEO600 100% Li ionomer[11] demonstrated that ionic aggregation becomes more extensive at high temperature, and so ionic conductivity is more hindered by extensive aggregation. At 35 wt% PEONPs, there is a discontinuity in conductivity near room temperature, where the grafted PEO5k chains begin to crystallize. Since segmental motion in the amorphous phase of PEO is responsible for ion conduction, σ_{DC} drops by an order of magnitude below room temperature, comparable to the neat ionomer.

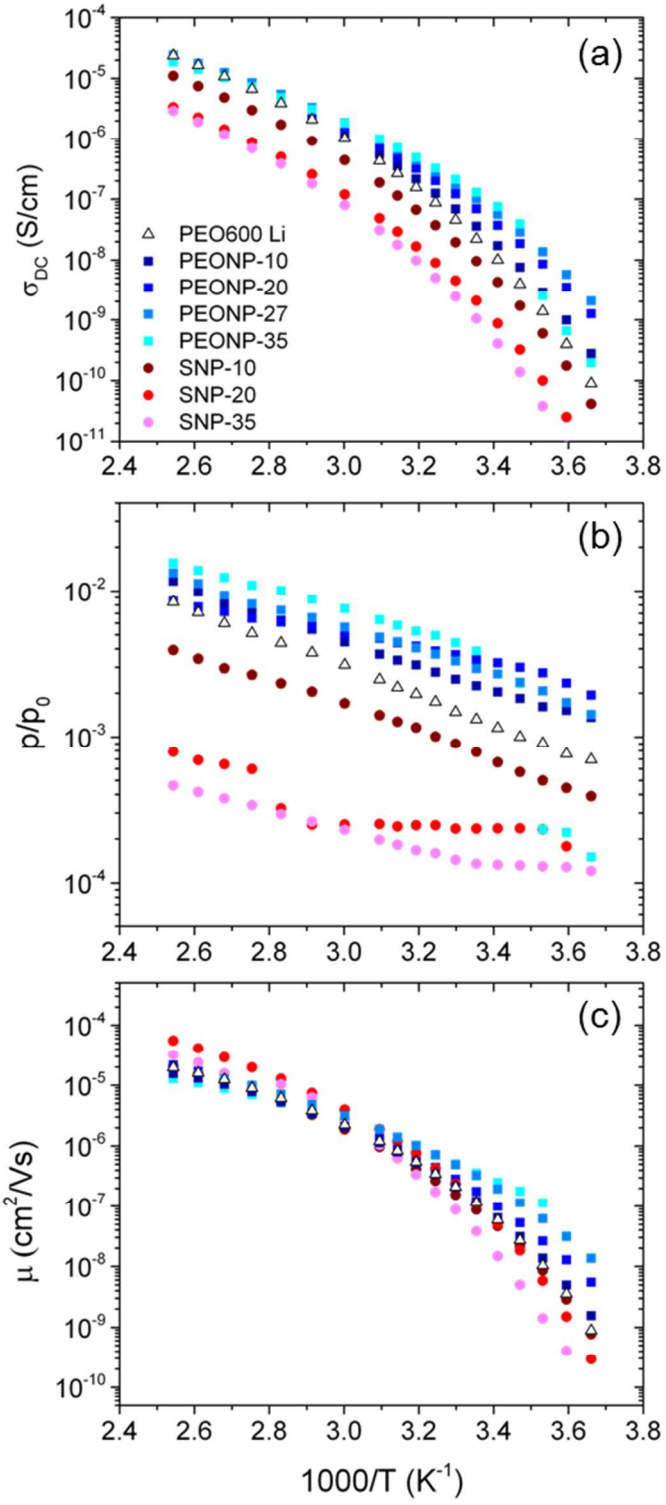

Figure 5. (a) DC conductivity, **(b)** conducting ion content normalized by the total ion content p_0, and **(c)** ionic mobility in PEONP (squares) and SNP (circles) ionomer nanocomposites obtained by DRS measurements and electrode polarization analysis.

The non-linear temperature response of σ_{DC} implies that an ionomer with a lower glass transition temperature should demonstrate better ion dynamics. DC conductivity improvements observed for PEONP nanocomposites at room temperature are well-explained by the reduction in glass transition temperature (Figure 5). The aggregated PEONP brushes provide a low T_g, ether oxygen-rich environment for facile ion conduction and we surmise that ion conduction is accelerated near PEONP clusters.

The ionic conductivity of bare silica nanocomposites decreases by more than an order of magnitude at 35 wt% silica compared with the neat ionomer. Hydrogen bonding between surface hydroxyls and ether oxygens effectively reduce the EO:Li ratio, leading to less ion solvation in the ionomer and slower ionic rearrangement timescales ($\tau_{\alpha 2}$), see Figure 7. Additionally, strong ionic interactions between $LiSO_3$ and surface hydroxyls will anchor ions in place, preventing them from exhibiting typical ionic relaxations.

Figure 8(b) clearly shows the difference in the number of simultaneously conducting ions normalized by the total ion content (p_0) between a nanocomposite containing PEONPs and SNPs. Adding PEONPs increases the conducting ion concentration, while adding SNPs decreases conducting ion concentration. Conducting ion concentration demonstrates linear temperature dependence on a log-linear scale, as observed previously.[9] The low glass transition temperature of the PEO ligands and the added ether oxygen content near the nanoparticle interface increase the number of mobile charge carriers. Our objective to increase the number of simultaneously conducting ions was successful in improving ionic conductivity. Lithium ion mobility (Figure 8(c)) in bare silica nanocomposites demonstrates stronger temperature dependence than PEONP nanocomposites. Plasticization with PEONPs cause the enhanced mobility at low temperature, but as seen in DC conductivity, PEO brushes do not improve ion transport at high temperature

due to poor solvation ability. Thus, the PEONPs dampen the temperature response of ion mobility at the highest weight fractions.

3.5. Viscoelastic Response

Viscoelastic measurements were made on SNP and PEONP nanocomposites to determine the nanoparticle's impact on viscosity and modulus of the nanocomposite (Figures 9(a) and 9(b)). The viscosity (η) of PEO600 100% Li exhibits liquid-like behavior. Consistent with the reduction in the glass transition temperature, all nanocomposites with increasing content of PEONPs maintain the liquid-like viscoelastic response of the neat ionomer. The low T_g associated with the PEONPs that aids conductivity leads to a reduction in viscosity, offering no mechanical advantage from these plasticizing nanoparticles. The viscosity reduction correlates well with the acceleration of the α_2 relaxation process, reduction in glass transition temperature, and increase in conductivity. As alluded to by the reduced ionic conductivity and good dispersion in the SNP nanocomposites, their viscosity increases. The viscoelastic response transitions from liquid to solid-like behavior with increasing SNP content, and varies independently of the glass transition. Segmental relaxations no longer dictate the rigidity of the nanocomposite and high SNP compositions resemble network structures caused by polymer bridging between SNPs, observable as the onset of a plateau in the complex modulus at low frequencies, Figure 9(b).[48] In this regime, modulus is influenced by SNP-polymer interaction, while unbound PEO ionomer chain segments contribute to the glass transition. At 35 wt% SNPs, the nanocomposite exhibits solid characteristics at 50 °C ($G^* > 10^5$ Pa) with a T_g below room temperature (-13 °C). Figure 9(c) plots the complex modulus at 1 Hz at 50 °C as a function of nanoparticle content for both PEONPs (blue) and SNPS (red). The gelation point occurs between

~10 and 20 wt% SNP, realized as an exponential increase in G^*, but more compositions would be necessary to determine a precise threshold.

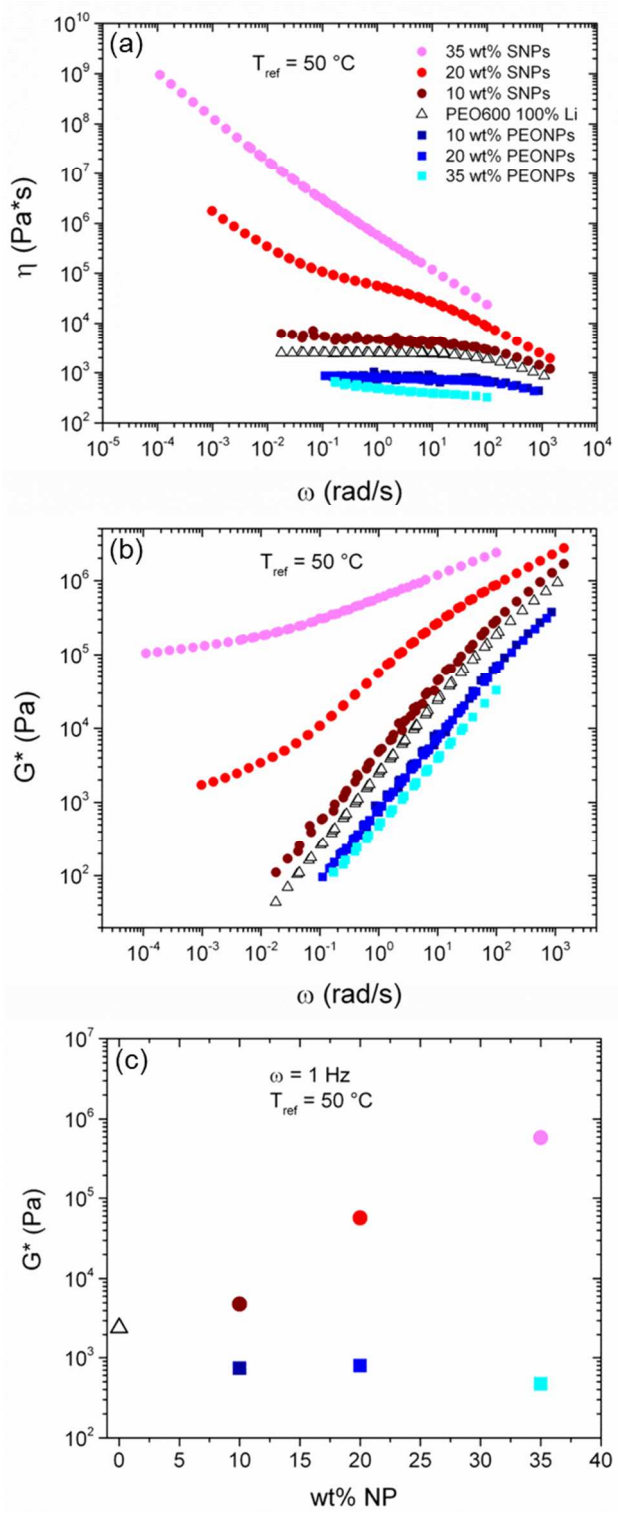

Figure 9. (a) Viscosity, η, and **(b)** complex modulus, G^*, of nanocomposite ionomers at a reference temperature of 50 °C. **(c)** G^* as a function of wt.% NP for each nanocomposite measured at 1 Hz at 50 °C. The legend provided in (a) applies to (b) and (c) as well.

The relationship between conductivity and viscosity are elucidated in a Walden plot, Figure 10, wherein $\log(\sigma_{DC})$ is linearly related to $\log(1/\eta)$.[49] All of the liquid-like samples can be described by a single linear fit between 30 °C and 90 °C (black dashed line, Figure 10), demonstrating that the ratio between conductivity and viscosity is independent of PEONP composition. Nanocomposites containing high SNP compositions (20 and 35 wt%) deviate from this common fit, because these concentrations of SNPs impose network formation. While conductivity is mildly inhibited by favorable interactions with silica surfaces, viscosity is significantly increased by gel formation. The white area in Figure 10 represents a desirable regime for these nanocomposite ionomers, where conductivity is higher than expected at a particular viscosity. Up to three orders of magnitude improvement in viscosity is achieved at the cost of just one order of magnitude in conductivity at any temperature for SNP-35. While the PEONPs plasticize the PEO ionomer to improve ionic conductivity with a commensurate decrease in viscosity, SNPs are capable of increasing viscosity with only a modest decrease in conductivity. Therefore, unlike traditional plasticizers, PEONPs can serve as non-volatile, ion-accelerating electrolyte plasticizers. Meanwhile, SNPs may perform more robustly for polymer electrolytes in battery applications where dendrite growth must be impeded by a robust separator. With these common battery design considerations in mind, it might be possible to use both nanoparticles in tandem to improve ion dynamics and mechanical performance.

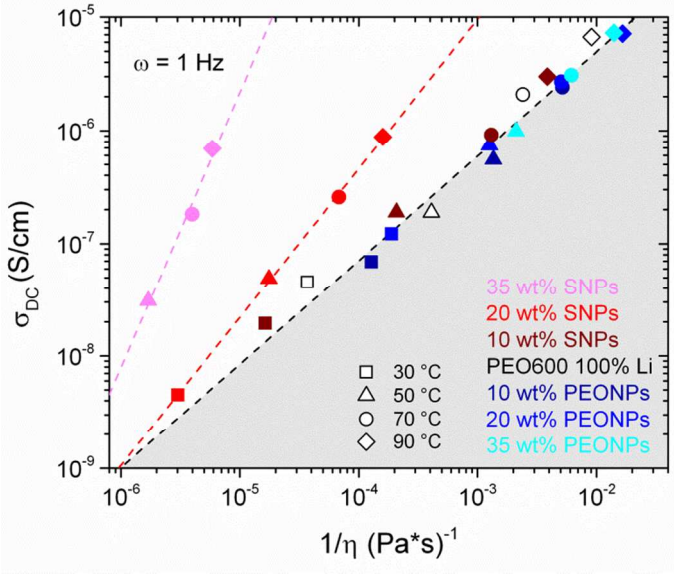

Figure 10. Walden plot demonstrating the linear relationship between DC conductivity and inverse viscosity across all temperatures. Dashed lines are linear fits to 35 wt% SNP (pink), 20 wt% SNP (red), and all other data points (black). The white area represents the desirable performance regime where viscosity is improved at low conductivity cost.

4. SUMMARY

Silica nanoparticles were grafted with dense brushes of high molecular weight polyethylene oxide and blended with a PEO-based single-ion conductor. Nanoparticle dispersion, ion transport, viscoelastic properties, and thermal properties of PEONP nanocomposites were compared with bare silica nanocomposites. Ionomer relaxations and ion transport properties were probed with dielectric spectroscopy and ion dynamics were correlated to T_g and viscosity.

The cardinal difference between SNPs and PEONPs is the interaction with the host ionomer. Surface hydroxyls of SNPs interact favorably with the PEO ionomer matrix to promote good dispersion and elevate viscosity. No change in glass transition is observed, but DC conductivity is reduced by an order of magnitude as $\tau_{\alpha 2}$ (ionic rearrangement) slows down. In contrast, PEONPs plasticize the ionomer, as evidenced by a drop in T_g with increasing PEONP

content, although PEONPs disperse poorly in the ionomer. Non-linear ionic conductivity signifies that ion transport is coupled to the segmental motion of the PEO ionomer, so the enhanced segmental dynamics near the ether oxygen-rich PEONP/ionomer interface provide facile conduction pathways for solvated ions at room temperature. The differences between SNP and PEONP viscoelastic properties demonstrate that SNPs might be useful for mechanical enhancement, as the conductivity deviates favorably from the viscosity-defined Walden line. Meanwhile, employing PEO-grafted nanoparticles as a solid plasticizer shows promise for improving ion dynamics in other ionomer systems.

5. ACKNOWLEDGEMENTS

The work is supported by the U. S. Department of Energy, Office of Science, Office of Basic Energy Sciences, under Contract No. DE-FG02-07ER46409. The authors acknowledge the Penn Nanoscale Characterization Facility for access to electron microscopy equipment, and the Materials Research Science & Engineering Centers (NSF MRSEC DMR – 1120901) for X-ray instrumentation. The authors thank Professors James Runt and Ralph Colby at Penn State University for thoughtful discussion and access to equipment, and thank Dr. U Hyeok Choi, Dr. Siwei Liang, Josh Bartels, and Dr. Ciprian Iacob for experimental assistance.

6. REFERENCES

1. J. B. Goodenough and K.-S. Park, *Journal of the American Chemical Society*, 2013, **135**, 1167-1176.
2. J. W. Fergus, *Journal of Power Sources*, 2010, **195**, 4554-4569.
3. S. K. Fullerton-Shirey and J. K. Maranas, *Journal of Physical Chemistry C*, 2010, **114**.

4. S. Takeoka, H. Ohno and E. Tsuchida, *Polym. Adv. Technol.*, 1993, **4**, 53-73.

5. W. Gorecki, M. Jeannin, E. Belorizky, C. Roux and M. Armand, *Journal of Physics: Condensed Matter*, 1995, **7**, 6823.

6. C. D. Robitaille and D. Fauteux, *Journal of the Electrochemical Society: Electrochemical Science and Technology*, 1986, **133**, 315-325.

7. J. M. Tarascon and M. Armand, *Nature*, 2001, **414**, 359-367.

8. S. Dou, S. Zhang, R. J. Klein, J. Runt and R. H. Colby, *Chemical Materials*, 2006, **18**, 4288-4295.

9. D. Fragiadakis, S. Dou, R. H. Colby and J. Runt, *J. Chem. Phys.*, 2009, **130**, 064907.

10. W. Wang, W. Liu, G. J. Tudryn, R. H. Colby and K. I. Winey, *Macromolecules*, 2010, **43**, 4223-4229.

11. W. Wang, G. J. Tudryn, R. H. Colby and K. I. Winey, *Journal of the American Chemical Society*, 2011, **133**, 10826-10831.

12. K. J. Lin and J. K. Maranas, *Macromolecules*, 2012, **45**, 6230-6240.

13. D. J. Roach, S. Dou, R. H. Colby and K. T. Mueller, *J. Chem. Phys.*, 2012, **136**.

14. K. Sinha, W. Q. Wang, K. I. Winey and J. K. Maranas, *Macromolecules*, 2012, **45**, 4354-4362.

15. H.-S. Shiau, W. Liu, R. H. Colby and M. J. Janik, *J. Chem. Phys.*, 2013, **139**, 204905.

16. M. V. O'Reilly, H. Masser, D. R. King, P. C. Painter, R. H. Colby, K. I. Winey and J. Runt, *Polymer*, 2015, **59**, 133-143.

17. U. H. Choi, S. Liang, M. V. O'Reilly, K. I. Winey, J. Runt and R. H. Colby, *Macromolecules*, 2014, **47**, 3145-3153.

18. J. Syzdek, M. Armand, M. Marcinek, A. Zalewska, G. Żukowska and W. Wieczorek, *Electrochim. Acta*, 2010, **55**, 1314-1322.

19. F. Croce, G. B. Appetecchi, L. Persi and B. Scrosati, *Nature*, 1998, **394**, 456-458.

20. F. Croce, R. Curini, A. Martinelli, L. Persi, F. Ronci, B. Scrosati and R. Caminiti, *J. Phys. Chem. B*, 1999, **103**, 10632-10638.

21. B. Scrosati, F. Croce and L. Persi, *Journal of the Electrochemical Society*, 2000, **147**, 1718-1721.

22. S. Srivastava, J. L. Schaefer, Z. Yang, Z. Tu and L. A. Archer, *Adv. Mater.*, 2014, **26**, 201-234.

23. P. R. Chinnam and S. L. Wunder, *Chem. Mat.*, 2011, **23**, 5111-5121.

24. P. R. Chinnam and S. L. Wunder, *Journal of Materials Chemistry A*, 2013, **1**, 1731-1739.

25. H. J. Zhang, P. Maitra and S. L. Wunder, *Solid State Ion.*, 2008, **178**, 1975-1983.

26. J. L. Nugent, S. S. Moganty and L. A. Archer, *Adv. Mater.*, 2010, **22**, 3677-+.

27. R. Rodriguez, R. Herrera, L. A. Archer and E. P. Giannelis, *Adv. Mater.*, 2008, **20**, 4353-4358.

28. J. L. Schaefer, D. A. Yanga and L. A. Archer, *Chem. Mat.*, 2013, **25**, 834-839.

29. X. W. Zhang, S. A. Khan and P. S. Fedkiw, *Electrochemical and Solid State Letters*, 2004, **7**, A361-A364.

30. X. W. Zhang and P. S. Fedkiw, *Journal of the Electrochemical Society*, 2005, **152**, A2413-A2420.

31. H. J. Zhang, X. W. Zhang, E. Shiue and P. S. Fedkiw, *Journal of Power Sources*, 2008, **177**, 561-565.

32. H. Zhang, X. Wei, K. Kopanski, E. Shiue and P. S. Fedkiw, *Advanced Science Letters*, 2011, **4**, 488-491.

33. P. A. Heiney, *Commission on Powder Diffraction Newsletter*, 2005, **32**, 9-11.

34. H. Hommel, A. P. Legrand, P. Tougne, H. Balard and E. Papirer, *Macromolecules*, 1984, **17**, 1578-1581.

35. K. Bridger and B. Vincent, *Eur. Polym. J.*, 1980, **16**, 1017-1021.

36. Y. Liu, M. H. Rafailovich, J. Sokolov, S. A. Schwarz, X. Zhong, A. Eisenberg, E. J. Kramer, B. B. Sauer and S. Satija, *Phys. Rev. Lett.*, 1994, **73**, 440-443.

37. C. Chevigny, F. Dalmas, E. Di Cola, D. Gigmes, D. Bertin, F. o. Boué and J. Jestin, *Macromolecules*, 2010, **44**, 122-133.

38. A. Bansal, H. Yang, C. Li, R. C. Benicewicz, S. K. Kumar and L. S. Schadler, *J. Polym. Sci. Pt. B-Polym. Phys.*, 2006, **44**, 2944-2950.

39. A. L. Frischknecht, *J. Chem. Phys.*, 2008, **128**.

40. J. Kim and P. F. Green, *Macromolecules*, 2010, **43**, 1524-1529.

41. M. J. A. Hore, A. L. Frischknecht and R. J. Composto, *Acs Macro Letters*, 2012, **1**, 115-121.

42. P. Maitra, J. Ding, H. Huang and S. L. Wunder, *Langmuir*, 2003, **19**, 8994-9004.

43. M. Wubbenhorst and J. v. Turnhout, *Journal of Non-Crystalline Solids*, 2002, **305**, 40-49.

44. S. Havriliak and S. Negami, *Journal of Polymer Science Part C: Polymer Symposia*, 1966, **14**, 99-117.

45. J. R. MacDonald, *Physical Review*, 1953, **92**, 4-17.

46. R. J. Klein, S. Zhang, S. Dou, B. H. Jones, R. H. Colby and J. Runt, *J. Chem. Phys.*, 2006, **124**, 144903.

47. G. J. Tudryn, M. V. O'Reilly, S. Dou, D. R. King, K. I. Winey, J. Runt and R. H. Colby, *Macromolecules*, 2012, **45**, 3962-3973.

48. M. Rubinstein and R. H. Colby, *Polymer Physics*, Oxford University Press, 2003.

49. P. Walden, *Z. phys. Chem*, 1906, **55**, 207-249.